AGU PUBLICATIONS

JGR

Journal of Geophysical Research: Atmospheres

RESEARCH ARTICLE
10.1002/2017JD027011

Key Points:
- Life cycle of contrail cirrus clusters controlled by synoptic situation and therefore very variable
- Lower initial ice crystal number concentration can initially cause larger contrail volume but radiative impact is nearly always reduced
- Mitigating the contrail cirrus climate impact by reducing soot number emissions is very efficient in large-scale ice-supersaturated areas

Correspondence to:
A. Bier,
andreas.bier@dlr.de

Citation:
Bier, A., Burkhardt, U., & Bock, L. (2017). Synoptic control of contrail cirrus life cycles and their modification due to reduced soot number emissions. *Journal Geophysical Research: Atmospheres*, *122*, 11,584–11,603. https://doi.org/10.1002/2017JD027011

Received 22 APR 2017
Accepted 28 SEP 2017
Accepted article online 6 OCT 2017
Published online 11 NOV 2017

Synoptic Control of Contrail Cirrus Life Cycles and Their Modification Due to Reduced Soot Number Emissions

A. Bier[1], **U. Burkhardt**[1], **and L. Bock**[1]

[1]Deutsches Zentrum für Luft- und Raumfahrt, Institut für Physik der Atmosphäre, Oberpfaffenhofen, Germany

Abstract The atmospheric state, aircraft emissions, and engine properties determine formation and initial properties of contrails. The synoptic situation controls microphysical and dynamical processes and causes a wide variability of contrail cirrus life cycles. A reduction of soot particle number emissions, resulting, for example, from the use of alternative fuels, strongly impacts initial ice crystal numbers and microphysical process rates of contrail cirrus. We use the European Centre/Hamburg (ECHAM) climate model version 5 including a contrail cirrus modul, studying process rates, properties, and life cycles of contrail cirrus clusters within different synoptic situations. The impact of reduced soot number emissions is approximated by a reduction in the initial ice crystal number, exemplarily studied for 80%. Contrail cirrus microphysical and macrophysical properties can depend much more strongly on the synoptic situation than on the initial ice crystal number. They can attain a large cover, optical depth, and ice water content in long-lived and large-scale ice-supersaturated areas, making them particularly climate-relevant. In those synoptic situations, the accumulated ice crystal loss due to sedimentation is increased by around 15% and the volume of contrail cirrus, exceeding an optical depth of 0.02, and their short-wave radiative impact are strongly decreased due to reduced soot emissions. These reductions are of little consequence in short-lived and small-scale ice-supersaturated areas, where contrail cirrus stay optically very thin and attain a low cover. The synoptic situations in which long-lived and climate-relevant contrail cirrus clusters can be found over the eastern U.S. occur in around 25% of cases.

1. Introduction

Aviation contributes around 5% to the anthropogenic radiative forcing (Lee et al., 2009). Because the aviation sector is forecast to grow yearly by about 5% (International Civil Aviation Organization, 2007), the aviation climate impact will increase significantly. Contrail cirrus, consisting of line-shaped contrails that form behind aircraft and the more irregularly formed cirrus clouds developing from them, are an important contributor. Radiative forcing due to contrail cirrus has been estimated to be larger than that due to CO2 emitted from air traffic and accumulated since the beginning of air traffic (Boucher et al., 2013; Burkhardt & Kärcher, 2011) making them an attractive target for mitigation options. Contrail cirrus ice crystals scatter the incident short-wave radiation, exerting a cooling. On the other hand, absorption and emission of longwave (LW) radiation reduce the terrestrial outgoing radiation significantly because absorbed infrared radiation is emitted at much lower temperatures than from the Earth's surface. This warming effect outweighs on average the cooling effect for optically thin cirrus clouds, such as contrails, and leads to a positive net radiative forcing at the top of the atmosphere (e.g., Meerkötter et al., 1999; Myhre et al., 2009; Williams & Webb, 2009). Burkhardt and Kärcher (2011) estimate a global net radiative forcing by contrail cirrus of 38 mW m^{-2} for the year 2002. An associated change in the natural cloudiness limits the radiative forcing to about 31 mW m^{-2} since the formation of natural cirrus is suppressed and their optical depth decreased by the presence of contrail cirrus due to the competition for the available water vapor and due to cloud diabatic heating.

Contrails form in sufficiently cold (mostly at temperatures below −45 to −50°C) and moist air when the Schmidt-Appleman criterion (Schumann, 1996) is fulfilled. At contrail formation, water supersaturation, larger than observed in the free atmosphere, is reached in aircraft exhaust plumes. Aerosol particles within the exhaust plume, in particular emitted soot but also ambient aerosol particles, act as condensation nuclei which activate into water droplets and subsequently freeze by homogeneous nucleation into ice crystals (Kärcher et al., 2015). Some aerosol particles may nucleate heterogeneously, depending on size, shape, and chemical composition. However, as long as plume air does not reach water saturation, contrails remain

subvisible and are therefore not considered in contrail cirrus parameterizations. Laboratory measurements imply that soot particles are not efficient ice nuclei (Bond et al., 2013) so that the majority of contrail ice crystals develop by homogeneous freezing of droplets. Young contrails differ from cirrus clouds mainly in terms of their microphysical properties. Within the aircraft plume, a large number of ice crystals form so that young contrails consist of a large number of small ice crystals (Kärcher et al., 1996; Petzold et al., 1997; Schröder et al., 2000).

The formation of natural cirrus requires highly ice-supersaturated regions (in case of homogeneous nucleation at relative humidities $\gtrsim$150%) (Koop et al., 2000). Ice-supersaturated areas generally develop in large-scale upward and often divergent motions cooling the air parcels due to vertical lifting (e.g., Irvine, Hoskins, & Shine, 2014; Gierens & Brinkop, 2012). Ice-supersaturated regions, identified in the European Centre for Medium-Range Weather Forecasts Re-Analysis Interim data over the North Atlantic region, frequently occur in jet stream and storm track regions and in locations of orographically-generated gravity waves (Irvine, Hoskins, & Shine, 2012). Large-scale motions in the extratropics are typically induced in baroclinic zones where optically thicker natural cirrus is often observed (e.g., Carlson, 1991). Ahead of these baroclinic zones, the upper tropospheric air is usually ice-supersaturated but cloud-free. Therefore, large fields of persistent contrails can develop in those environments identified as contrail outbreaks (Carleton et al., 2008; Schumann, 2005). Two common meteorological situations leading to contrail outbreaks are (a) a slow ascent of upper air ahead of a surface warm front and (b) strong winds ahead of a surface cold front in more convective and turbulent regions (Kästner, Meyer, & Wendling, 1999).

The life cycle of contrail cirrus has been studied in observations and model simulations. Contrail detection algorithms have been applied to satellite images (Minnis et al., 2013; Palikonda et al., 2005), and contrails have been tracked automatically (Vazquez-Navarro, Mannstein, & Kox, 2015). The detection of contrail cirrus by satellite instruments is often constrained to young and line-shaped contrails of relatively high optical depth. The optical depth of contrail cirrus often lies below the threshold of the detection algorithms (e.g., Duda et al., 2013; Kärcher et al., 2009), or the difference of the brightness temperature of contrails and underlying clouds may be too small prohibiting detection. The life cycle of contrail cirrus is highly variable with many contrails living for a short time, never losing their initial linear shape (Vazquez-Navarro et al., 2015), and some contrails forming impressive clusters of contrail cirrus that are immediately obvious in satellite images (Duda et al., 2004; Duda, Minnis, & Nguyen, 2001; Haywood et al., 2009).

The development of young contrails and the transition to contrail cirrus are often studied in detail within an idealized background atmosphere using large eddy simulations (LES) (e.g., Lewellen, Meza, & Huebsch, 2014; Paoli & Shariff, 2016; Picot et al., 2015; Unterstrasser & Gierens, 2010a, 2010b). Large-scale models are used to study the global radiative forcing of contrail cirrus prescribing a global emission data set (e.g., Bock & Burkhardt, 2016a; Burkhardt & Kärcher, 2011; Chen & Gettelman, 2013; Schumann et al., 2015). In those simulations new contrails constantly form, perturbing the already existing contrail cirrus, so that the contrail cirrus life cycle, the processes that control them, and their dependency on the synoptic situation can be only analyzed indirectly (Newinger & Burkhardt, 2012).

Contrail cirrus life cycles have been studied using a contrail cirrus parameterization within the European Centre/Hamburg (ECHAM) climate model, version 5 (ECHAM5-CCMod), prescribing air traffic locally and for a limited time (e.g., Bock & Burkhardt, 2016a; Burkhardt & Kärcher, 2009) so that simulated contrails all have the same age and are formed within a particular synoptic regime. ECHAM5-CCMod was shown to simulate a life cycle of contrail cirrus in line with findings from LES. An initial increase in contrail optical depth is connected with a large increase in contrail ice water path. The subsequent decline of the optical depth results from the strong dilution and the associated decline in ice crystal number concentrations and ice water content. Whereas LES are suited to studying contrail life cycles due to their high resolution and detailed microphysical schemes, the climate model is able to simulate the major features of the contrail cirrus life cycle and its interaction with the synoptic variability.

Contrail cirrus properties can be influenced by changing aircraft emissions, either by introducing a next generation of cleaner aircraft engines or by using alternative fuels. Box model studies as well as ground and flight measurements have shown that the emitted soot particle number is significantly reduced by the use of alternative fuels such as Fischer-Tropsch (FT) fuels based on coal or natural gas or biofuels like hydroprocessed esters and fatty acids (Beyersdorf et al., 2014; Moore et al., 2015, 2017; Rojo et al., 2015; Speth et al., 2015).

Measurements of contrails using a 50:50 blend of FT and conventional kerosene (ACCESS and ECLIF-I) indicate a reduction in in-flight soot number emissions by 50%–70% (Moore et al., 2017) and in the initial ice crystal number by around 50% (C. Voigt, personal communication). There are several possibilities to reduce soot number emissions further, for example, using pure alternative fuels or a blend with a lower aromatics content, using bio kerosene together with liquid natural gas/liquid hydrogen (Grewe et al., 2016), or improving engine designs like going toward lean combustion. A reduction of soot number emissions leads to a lower initial ice crystal number concentration at contrail formation because of the decrease in the number of available condensation nuclei. Assuming a reduction of current soot number emissions (around $5 \cdot 10^{14}$–10^{15} kg-fuel^{-1}) by 50%, the initial ice crystal number at contrail formation is reduced by the same magnitude as long as the atmospheric state is not close to the contrail formation threshold (Kärcher et al., 2015; Kärcher & Yu, 2009). Otherwise, the initial ice crystal number is constrained by the lower supersaturation within the plume and not by the aerosol particle number. The vortex phase tends to decrease the differences in ice crystal formation between current and reduced soot number emissions due to the sublimation of ice crystals within the sinking vortices (Unterstrasser, 2016).

In this paper, we study the life cycle of several simulated contrail cirrus clusters within different synoptic situations. Our aim is to analyze the variability of contrail cirrus life cycles, the importance of microphysical and dynamical processes responsible for this variability, and the impact of a change in initial ice crystal number depending on the synoptic situation. Exemplarily, we investigate the influence of an 80% reduction in initial ice crystal number. For selected cases, we perform sensitivity experiments prescribing different reductions. In section 2, we introduce the ECHAM5-CCMod climate model describing the setup of our simulations and the diagnostics. We conduct idealized process studies, prescribing air traffic only over the eastern U.S. in winter time at 260 hPa for only 1 h, and analyze the development of the resulting contrail cirrus clusters. We choose the eastern U.S. since it is one of the peak air traffic areas where contrail cirrus outbreaks can be frequently seen. In section 3, the evolution of a long-lived contrail cirrus cluster in a long-lived and large-scale ice-supersaturated area is described in detail. The dynamical and microphysical processes, determining the temporal evolution of contrail cirrus properties and limiting the lifetime of the contrail cirrus cluster, are analyzed. After this in-depth analysis, we study the variability of life cycles depending on the synoptic situation in section 4. The dependency of dynamical and microphysical process rates on the synoptic situation and on the initial ice crystal number is studied in order to improve our understanding of the processes determining contrail cirrus life cycles. We analyze whether contrail cirrus life cycles are mainly controlled by microphysical or dynamical processes and discuss the effect of reduced soot particle emissions in the different cases. We investigate in which type of synoptic situation the influence of soot number emissions on contrail cirrus properties, life cycle, and radiative impact, in terms of "total extinction," is largest. Finally, in section 5, we study the frequency of synoptic situations supporting long-lived and climate-relevant contrail cirrus clusters. A summary and conclusions are given in section 6.

2. Model and Methods

2.1. ECHAM5-CCMod

We use the contrail cirrus modul (CCMod) within the German community atmospheric circulation model ECHAM5-HAM. ECHAM5 is the fifth generation of the general atmospheric circulation model ECHAM (Roeckner et al., 2003; Roeckner et al., 2006). ECHAM5 has been extended by the aerosol module HAM (Stier et al., 2005). The cloud scheme in ECHAM5 is based on the diagnostic cloud cover scheme by Sundqvist (1978) which calculates fractional cloud coverage from grid-mean relative humidity (relative humidity scheme) assuming a uniform probability density function for the subgrid scale variability of total water. ECHAM5 includes a microphysical two-moment scheme (Lohmann et al., 2008) adapted in the ice cloud regime to be used in combination with the fractional cloud coverage scheme. The fractional ice-supersaturated area is parameterized consistent with the cloud scheme and has been evaluated using observational data (Bock & Burkhardt, 2016b; Burkhardt et al., 2008; Lamquin et al., 2012).

The contrail cirrus scheme CCMod is based on the parameterization by Burkhardt and Kärcher (2009) and was extended by Bock and Burkhardt (2016a) to a microphysical two-moment scheme. The microphysical two-moment scheme allows a more realistic representation of the microphysical processes and properties and their change due to a reduction in soot number emissions. Contrail cirrus is treated as a separate cloud

class. CCMod comprises of prognostic equations for the fractional contrail cirrus cover, volume, contrail cirrus length, ice water content, and ice crystal number concentration (Bock & Burkhardt, 2016a). Contrails form in the fractional area of a grid box in which the Schmidt Appleman criterion (Schumann, 1996) is fulfilled and persist in the fractional area of the grid box that is ice-supersaturated but cloud-free (Burkhardt et al., 2008). The processes affecting contrail cirrus coverage and properties, such as contrail formation below a threshold temperature, volume growth due to turbulent diffusion, and sedimentation and tilting due to vertical wind shear, are parameterized. Natural cirrus and contrail cirrus can interact by competing for available water vapor and by heating the atmosphere and thereby changing the relative humidity (Burkhardt & Kärcher, 2011).

Microphysical processes, in particular sedimentation and precipitation, are parameterized in the same way as for natural cirrus clouds. Sedimentation is treated as vertical advection (Roeckner et al., 2003), and the fall velocity is calculated depending on the average ice crystal mass (Heymsfield & Iaquinta, 2000; Spichtinger & Gierens, 2009). Contrail cirrus ice crystals can precipitate when ice crystals aggregate to snowflakes (Murakami, 1990) or when contrail cirrus ice crystals are collected by already falling snowflakes (Levkov et al., 1992; Lin, Farley, & Orville, 1983). Water vapor deposition is parameterized dependent on the ice crystal number concentration. In the presence of high in-cloud ice crystal number concentrations, we apply saturation adjustment relaxing ice supersaturation within the contrail volume within one time step (Bock & Burkhardt, 2016a). This is in particular the case for young contrails since ice crystal number concentrations are, in general, very large (Heymsfield, Lawson, & Sachse, 1998). In aged contrails and in areas below the contrail core, which receive ice crystals due to sedimentation, water vapor deposition may be limited by low ice crystal number concentrations.

2.2. Experiments and Model Setup

We study the temporal evolution of contrail cirrus clusters prescribing air traffic for 1 h only over the eastern U.S. (34–44°N and 85–100°W) at a specified pressure level (260 hPa or 220 hPa). By restricting air traffic to one location and a short time period, we are able to analyze the life cycle of a cluster of contrail cirrus (all of the same age) developing in a specific synoptic situation. We analyze the contrail formation and development in 10 synoptic situations in January varying the flight level and the initial ice crystal number concentration of contrails. We select winter time because the synoptic variability in this latitudinal region is larger in winter than in summer due to an increased activity within the storm tracks.

Contrails formed in 8 of the 10 synoptic situations. Based on aircraft measurements of 5–10 min old contrails (Febvre et al., 2009; Schröder et al., 2000; Schumann, 2002; Voigt et al., 2010), we initialize contrails with a cross-sectional area of 40,000 m^2 and an ice crystal number concentration of 150 cm^{-3} (Bock & Burkhardt, 2016a), resulting in an initial ice crystal number per flight distance of $6 \cdot 10^{12}$ m^{-1}, at a contrail age of 7.5 min. This initial ice crystal number is regarded typical for current fuels and engines and represents the "high soot emissions" in this paper. The impact of reduced soot number emissions is approximated by a reduction of the initial ice crystal number in the same magnitude. Exemplarily and in order to obtain significant changes in contrail cirrus properties and life cycles, we reduce the initial ice particle number concentration by 80% to 30 cm^{-3}, leading to an initial ice crystal number of $7.5 \cdot 10^{11}$ m^{-1} representing the "low soot emissions." In addition, we study the sensitivity of the short-wave radiative impact by contrail cirrus to further reductions in the initial ice crystal number for two synoptic cases. We compare the life cycle of contrail cirrus for high and low soot emissions starting from a specified initial atmospheric state. We find that the two simulations are directly comparable because the background meteorology is not significantly altered, within the simulation period, due to the differences in the contrail initialization. In our simulation of a large contrail cirrus outbreak, we find locally maximum deviations in temperature of 0.03 K and in total water mixing ratio of 4.1% after 12 h between the two simulations, which does not affect the contrail cirrus life cycle substantially.

To study the frequency of synoptic situations supporting long-lived and climate-relevant contrail cirrus clusters, we additionally ran the model for two whole years prescribing air traffic at 220 hPa in the same region every 28 h, in order to rotate through the diurnal cycle.

We perform simulations at a horizontal resolution of T42. This corresponds to 2.8° by 2.8° on a Gaussian grid or around 300 by 300 km at the equator. The model has 41 vertical levels leading to a layer thickness of about 500 m in the upper troposphere and lowermost stratosphere (Kurz, 2007), where contrails mainly develop.

The time step of the model is 15 min. Air traffic for the year 2002 is defined using the AERO2k flight inventory (Eyers et al., 2004).

2.3. Diagnostics

We analyze contrail cirrus life cycles in detail evaluating dynamical and microphysical process rates. We compare in particular the ice crystal number but also ice water budgets distinguishing ice crystal loss due to microphysical processes and due to dynamical reasons.

An important microphysical process, affecting the evolution of contrails, is the sedimentation of ice crystals. Ice crystal loss due to sedimentation occurs only if contrail ice particles fall into a dry, subsaturated layer and subsequently sublimate. We call this process "sedimentation loss." Precipitation is only of minor importance in contrail cirrus due to their typically low ice water content.

Dynamical reasons for ice crystal loss are transport of contrail cirrus into dry, ice-subsaturated areas or a drying of the air volume, in which contrails persist, causing ice crystal sublimation. We call this process "dynamical loss." Another process is the "replacement by natural cirrus." If humidity rises despite the presence of contrail cirrus, natural cloud cover increases and new ice crystals nucleate. If those new ice crystals form in the area where contrails persist, they mix with the contrail cirrus ice crystals. It is not clear if such clouds should be termed contrail cirrus or natural cirrus. We regard them as natural clouds and call the associated process "replacement of contrail cirrus by natural cirrus."

We define "total extinction" of contrail cirrus similarly to Unterstrasser and Gierens (2010a). Extinction, a dimensionless quantity, is a measure for the disturbance in incident short-wave radiation by scattering and reflection within one column. Assuming a solar zenith angle of 0°, the extinction of contrail cirrus can be expressed as $1 - \exp(-\tau_{cc})$, where τ_{cc} is the contrail cirrus optical depth which is defined as the vertical integral over the extinction coefficient (χ in m^{-1}) $\tau_{cc} = \int \chi(z) dz$. For small optical depth, extinction can be approximated by $1 - (1 - \tau_{cc}) = \tau_{cc}$. The total extinction is defined as the integral of the extinction over the area of the contrail cirrus cluster dA_{cc}

$$E_{cc} = \iint (1 - \exp(-\tau_{cc}(x,y)))dA_{cc} \approx \iint \tau_{cc}(x,y)\, dA_{cc} \tag{1}$$

and has the unit m^2. Discretized to model grid boxes equation (1) can be written as

$$E_{cc} = \Sigma_{x,y} \tau_{cc}(x,y)^* b_{cc}(x,y)^* A_{GB}(x,y), \tag{1a}$$

with *bcc* indicating fractional contrail cirrus coverage, A_{GB} the model grid box area, and *x* denoting longitude and *y* latitude. The total extinction can be interpreted as the product of the characteristic optical depth and the contrail cirrus cover and is a measure for the short-wave radiative impact due to contrail cirrus. Both optical depth and contrail cirrus cover are defined here assuming a vertically homogeneous distribution of contrail cirrus variables within a model level.

Total extinction is independent of time of day, and therefore the zenith angle of the Sun, cloud overlap, surface conditions, and other factors influencing radiative forcing. This is of advantage when analyzing contrail cirrus life cycles since total extinction can be compared directly and linked to microphysical and dynamical processes. To first order, a higher total extinction leads to a higher net radiative warming by contrail cirrus. Nevertheless, total extinction cannot replace an estimate for radiative forcing as the radiative forcing of contrail cirrus can be strongly modified by, for example, cloud overlap with natural clouds.

This relationship between net radiative forcing and total extinction is nonlinearly dependent on ice crystal size for fixed ice water content (e.g., Meerkötter et al., 1999; Zhang, Macke, & Albers, 1999). Analyzing this relationship within the ECHAM4 model, maximum radiative forcing for the simulated ice water content was found at ice crystal radii of about 9–12 μm (Marquart et al., 2003) staying relatively constant down to an ice crystal size of 6 μm. Since short-wave radiative forcing is reacting more strongly to the decrease in ice crystal size, net radiative forcing is decreased for smaller radii. The maximum of net radiative forcing is shifted toward smaller ice crystal sizes for lower ice water content. In our contrail cirrus life cycle experiments, both, ice water content and ice crystal sizes are initially very small increasing with time. Therefore, the relationship between short-wave and net radiative forcing holds in our experiments also for smaller ice crystal sizes since the ice water content is reduced at the same time. Anyway, total extinction should be only seen as an indicator for a large climate impact.

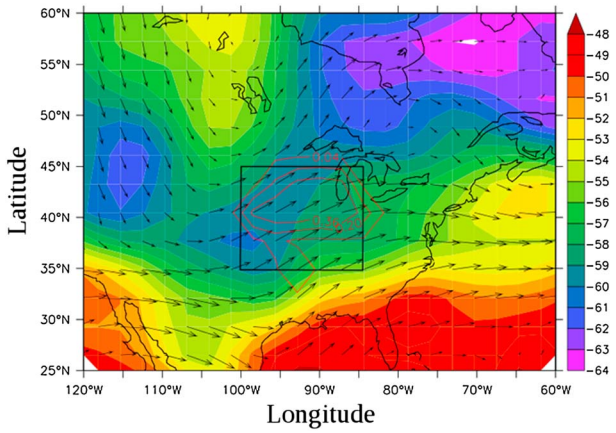

Figure 1. Contrail cirrus case study (case 1): synoptic situation with temperature (°C) (colors) and horizontal wind (arrows) as well as fractional contrail cover in percent (red contour lines) at 260 hPa right after termination of air traffic. The location of initialized air traffic (35°N–45°N, 85–100°W) is indicated by the black box. At the time of air traffic termination, parts of the contrail cluster have been already advected out of the black box.

Dividing total extinction by the initial contrail cover $A_0 = \sum_{x,y} b_{cc,0}(x,y)^* A_{GB}(x,y)$, determined at the last time step of contrail formation when air traffic is terminated, we obtain the "normalized total extinction"

$$E_{cc,N} = E_{cc}/A_0. \tag{1b}$$

The normalized total extinction is a measure for the short-wave radiative impact per initially formed contrail cover. By removing the dependency of total extinction on the initially formed contrail cover, we can distinguish between contrail cirrus clusters that have a large short-wave radiative impact due to their large extent and those that support only a small contrail volume but which are connected with a large increase in contrail optical depth.

We also calculate normalized contrail cirrus volume, dividing the contrail cirrus volume by the initial volume at the last time step of contrail formation.

3. Case Study of a Long-Lived Contrail Cirrus Cluster

We study the evolution of a contrail cirrus cluster in a particularly humid, large-scale, and long-lived ice-supersaturated area in detail before investigating the variability of life cycles depending on the synoptic situation. Figure 1 displays the synoptic situation, temperature, and horizontal wind at 260 hPa, and the contrail cirrus coverage over Northern America and the western part of the Atlantic at the start of the contrail cirrus life cycle. The wind field shows the position of an upper tropospheric trough at about 105°W, west of the Great Lakes. Downstream of the trough, the ridge axis is situated at about the east coast of the U.S. and Canada (~75°W). In the midlatitudes between 35°N and 45°N, temperatures at 260 hPa are relatively low, between −60°C and −55°C, in the area of the trough, with temperatures increasing to values between −55°C and −52°C toward the ridge. The region where air traffic is prescribed (black box) is located ahead of the trough axis. This is a humid region with a strong vertical updraft suitable for contrail formation and persistence. Specific humidity is low downstream of the ridge axis (southeast of the Great Lakes) due to subsidence.

3.1. Life Cycle for Current High Soot Emissions

The temporal evolution of a contrail cirrus cluster containing numerous individual contrails is shown in Figure 2. Some contrails in the cluster may be short-lived and others long-lived, depending on the background atmospheric conditions. First, we discuss the life cycle of the contrail cirrus cluster resulting from current soot number emissions.

3.1.1. Ice Particle Number

Figure 2a shows the total ice particle number of the whole contrail cirrus volume and the mean ice crystal number concentration. The total ice particle number decreases faster at the beginning and more slowly toward the end of the contrail cirrus life cycle. After 4 h, about 60% of the initially formed ice crystals are lost and total ice crystal number has declined by more than 1 order of magnitude after 10 h of age. Compared to the total ice crystal number, the ice crystal number concentration decreases much faster at the beginning of the life cycle due to the dilution of the contrail cirrus cluster; the reduction is more than 80% after 2 h already.

3.1.2. Volume and Ice Water Mass

The volume of contrail cirrus cluster with $\tau > 0.02$ (Figure 2c) grows strongly, at the beginning mostly due to turbulent diffusion and later mainly due to ice crystal sedimentation, increasing by a factor of 10 relative to the volume right after contrail formation and reaching its maximum at 6.5 h of age. At that time, only about 15% of the ice crystals survive. Ice water mass (Figure 2b) reaches its maximum at the same time as the volume.

The mean ice water content (Figure 2b) only slightly increases at the beginning of the life cycle reaching its maximum after about 1.5 h. This initial increase likely results from the production of ice supersaturation due to the large-scale lifting ahead of the trough. The decrease afterward is connected with the dilution associated with the increase in contrail cirrus volume. The decrease in contrail cirrus ice water mass and volume (connected with $\tau > 0.02$) after 6.5 h is due to the severely diminished ice crystal number and the therefore

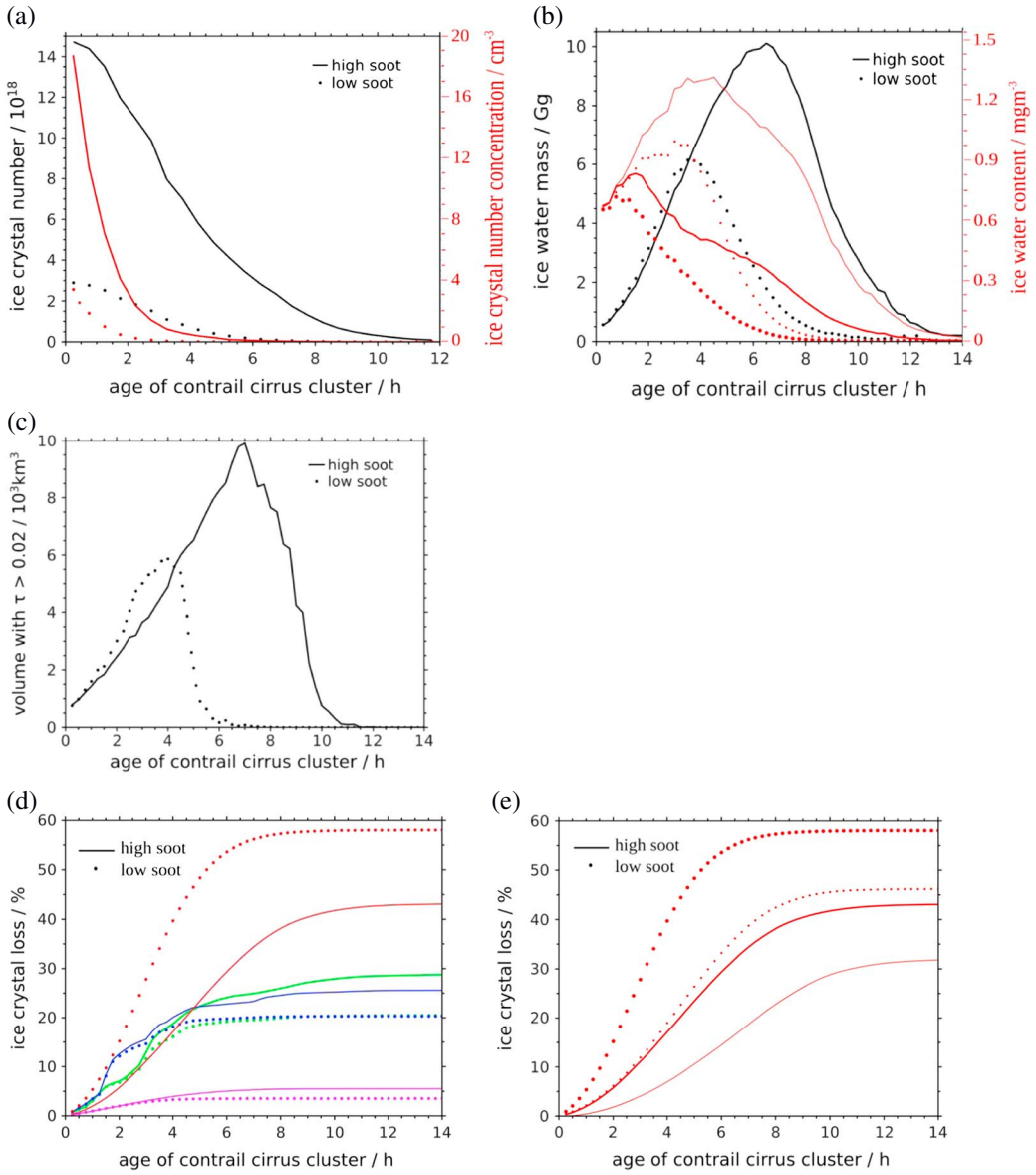

Figure 2. Temporal evolution of a contrail cirrus cluster showing contrail cirrus (a) total ice crystal number (black) and mean in-cloud ice crystal number concentration (red); (b) total ice water mass (black) and mean in-cloud ice water content (red) averaged over all vertical levels (thick) and only over the air traffic level (thin); (c) total volume with optical depth >0.02; (d) accumulated ice crystal loss in percent due to sedimentation (red), precipitation (purple), dynamical processes (green), and replacement by natural cirrus (blue) for air traffic at 260 hPa; and (e) ice crystal loss due to sedimentation for air traffic at 220 hPa (thin) and 260 hPa (thick). The solid lines represent the high soot, and the dotted lines represent the low soot case. The age of the contrail cirrus cluster indicates the time after the termination of air traffic. The flattening out of the curves indicates the end of the life cycle of the contrail cirrus cluster. The green dotted line in Figure 2c is partially hidden behind the blue dotted line.

limited deposition (Bock & Burkhardt, 2016a). The decreasing ice crystal number concentration leads to a low contrail cirrus optical depth and therefore to a severely decreased contrail cirrus volume with optical depth above a certain threshold.

3.1.3. Ice Crystal Loss Processes

Figure 2d shows the ice crystal loss accumulated over time due to the dynamical and microphysical processes as defined in section 2. In the southern part of the ice-supersaturated area, relative humidity is strongly increasing within the first 4 h of the contrail cirrus life cycle. This leads to an increase in natural cirrus coverage and to a decrease in cloud free ice-supersaturated area. Since our model cannot resolve a mix of contrail cirrus ice crystals with ice crystals from natural cirrus, we simulate a loss of contrail cirrus ice crystals due to

replacement by natural cirrus. At an age of about 4.5 h, 2 h before contrail cirrus volume (with $\tau > 0.02$) is largest, the loss of ice crystals due to sedimentation, due to dynamical reasons, and due to replacement by natural clouds is equal in size and amounts to about 20% each. After about 4.5 h, it is mainly the loss due to sedimentation that is continuing to increase since ice water mass and therefore ice crystal sizes have increased significantly. Accumulated over the whole life cycle of the contrail cirrus cluster, 43% of ice crystals are lost due to sedimentation; 28% sublimate due to large-scale advection into a dryer, ice-subsaturated region, mainly at the east coast of the U.S.; and 25% are lost due to replacement by natural cirrus mainly in the southern part of the cluster. Precipitation is generally of little importance in winter and accounts here for only 5% of ice crystal loss.

3.2. High Soot Versus Low Soot Emissions

In the following, we investigate the influence of the reduction of the initial ice crystal number by 80% on properties and life cycle of the contrail cirrus cluster. Qualitatively, the development of the contrail cirrus cluster is similar in the low soot and high soot case.

3.2.1. Ice Particle Number

Total ice particle number (Figure 2a) decreases faster at the beginning and more slowly in the later phase of the life cycle. The mean ice crystal number concentration (Figure 2a) declines much faster than the total ice particle number due to dilution at the beginning of the life cycle. Less than 1% of the initially formed ice crystals are left in the low soot case after 8 h, whereas in the high soot case the same fraction survives as long as about 11 h.

3.2.2. Volume and Ice Water Mass

The maximum contrail cirrus volume (Figure 2c) occurs in the low soot case 3 h earlier. While the maximum volume is only about 60% as large as in the high soot case, the contrail cirrus volume is larger in the low soot case at an age between 1 and 4 h. This initially stronger volume increase in the low soot case is caused by the faster increase in ice crystal sizes due to the lower initial ice crystal number while the amount of water vapor available for deposition is constant. This leads to an earlier and stronger increase in the sedimentation rate in the low soot case (Figure 2d). The vertical tilting (or spreading) of contrails due to vertical wind shear is proportional to the vertical extent of the contrails which is increased due to sedimentation and, in a more strongly sheared contrail, sedimentation leads to a larger volume increase. Therefore, the interaction between shear and sedimentation reinforces the earlier volume growth in the low soot case. Due to the larger contrail cirrus volume, more water vapor is available for deposition since in the early phase of the contrail cirrus life cycle deposition is only limited by the contrail cirrus volume (Bock & Burkhardt, 2016a). This stronger deposition again reinforces larger sedimentation rates and the increase in contrail cirrus volume. The later rapid decline in contrail cirrus volume (connected with an optical depth >0.02) after about 4 h in the low soot case is due to the severely diminished ice crystal number concentration and the therefore limited deposition rates (Bock & Burkhardt, 2016a). This decline is happening much earlier than in the high soot case.

Differences in contrail cirrus total ice water mass (Figure 2b) between the high and low soot case are similar to those for volume. In the low soot case, contrail cirrus contain initially slightly more ice water mass due to the larger contrail cirrus volume. After about 4 h, the ice water mass in the contrail cirrus cluster in the low soot case starts being lower than in the high soot case. Ice water mass is decreased below its value at the beginning of the life cycle (15 min of age) after 8 h while this happens for the high soot case after 12.5 h leading to an approximated lifetime difference of 4.5 h between high and low soot cases.

The mean ice water content (Figure 2b) for reduced soot emissions is approximately as large as for high soot emissions for the first hour of the contrail cirrus life cycle. Ice water content is strongly affected by dilution and sedimentation and quickly decreases while the total ice water mass is still increasing. The ice water content within the contrail core (at the level of air traffic), which is not affected by the volume increases due to sedimentation, increases for about 3–5 h, similar to the evolution of ice water mass.

3.2.3. Ice Crystal Loss Processes

Ice crystal loss is increased in the low soot case due to the strongly increased sedimentation rate (Figure 2d). At the end of the life cycle of the contrail cirrus cluster, 58% of ice particles are lost due to sedimentation, 15% more than in the high soot case. Both, ice crystal loss due to dynamical reasons and due to replacement by natural cirrus is decreased in the later part of the contrail cirrus life cycle, after about 3 h. This is likely due to the fact that at this time ice crystal loss due to sedimentation is already increased by more than 10%.

3.3. Upward Shift of Air Traffic

We repeated the high and low soot simulations prescribing air traffic at 220 hPa rather than 260 hPa in order to test the sensitivity of a long-lived contrail cirrus life cycle to the altitude. The two pressure levels mainly differ regarding the amount of water vapor available for deposition and additionally due to different advection speeds. In a large-scale and long-lived ice-supersaturated area, the vertical shift of air traffic affects the sedimentation processes similarly to the change of the soot number emissions. Figure 2e compares the associated sedimentation loss when prescribing air traffic at those two air traffic levels. Sedimentation is weaker and starts later when initializing the contrail cirrus cluster at the higher flight level because of the smaller amount of available water vapor in the upper troposphere and the associated lower ice crystal growth rates. Furthermore, dynamic loss rates may be increased due to slightly larger advection speeds. Accumulated over the whole life cycle, this leads to an 11% lower sedimentation loss than for air traffic at 260 hPa in the high soot case. Furthermore, the lifetime of the contrail cirrus cluster is increased at the higher flight level because ice particle loss due to sedimentation occurs more slowly. The differences in sedimentation loss due to the change in soot emissions at the two flight levels amount to about 15% both at 220 hPa and at 260 hPa.

In conclusion, ice crystal sedimentation into ice-subsaturated layers can be the most important ice crystal loss process in a large-scale and long-lived ice-supersaturated area. A reduction of the initial ice crystal number enhances sedimentation rates and leads initially to larger contrail cirrus volumes and cover and to a decrease in the lifetime of the contrail cirrus cluster. The reduction of soot emissions increasing the ice crystal loss due to sedimentation can be similarly effective for different air traffic levels.

4. Dependency on Synoptic Situation

The synoptic situation described above is very favorable for the formation and development of a long-lived and climate-relevant contrail cirrus cluster. However, many less favorable synoptic situations exist in which contrail cirrus life cycles are predominantly controlled by dynamical processes like the advection of ice crystals into dryer regions. Therefore, we performed nine additional simulations for randomly selected synoptic situations in winter prescribing air traffic at 260 hPa over the eastern U.S. For each of the synoptic situations we perform one simulation with high soot emissions and one with low soot emissions starting the two simulations with exactly the same atmospheric state. Since in 2 of the altogether 10 situations no contrails were formed, we investigate contrail cirrus properties, life cycle, and short-wave radiative impact for eight synoptic cases including the long-lived contrail cirrus cluster described above.

We define the following criterion to classify contrail cirrus life cycles based on the simulations when prescribing high soot emissions. We categorize a contrail cirrus cluster to be strongly microphysically controlled when more than 20% of ice crystals are lost due to sedimentation integrated over the whole life cycle. If less than 10% are lost due to sedimentation, we call the contrail cluster to be dynamically controlled and the transition regime is in between those two cases. Microphysically controlled contrail cirrus life cycles are typically associated with long-lived and large-scale ice-supersaturated areas. Dynamically controlled contrail cirrus clusters generally occur in short-lived and small-scale ice-supersaturated areas since contrail ice crystals are quickly transported into subsaturated areas. Table 1 includes a short description of the synoptic situations at the beginning of each contrail cirrus life cycle for the eight cases in which contrails form. The three microphysically controlled contrail cirrus clusters develop ahead of a trough which is a typical situation where persistent contrails are frequently observed (Kästner et al., 1999). One of the dynamically controlled situations is connected with high natural cirrus cloud coverage. The second dynamically controlled case and one situation in the transition regime occur within a zonal flow in a dry and cold air mass. The remaining contrail cirrus clusters in the transition regime evolve within or even ahead of a ridge.

We first discuss the life cycle of one dynamically controlled case and then compare the temporal evolution of contrail cirrus clusters for the eight synoptic situations. The classification of the eight case studies, in which contrails form, is given in Table 1.

4.1. Dynamically Controlled Life Cycle

Figure 3 shows the temporal evolution of total ice crystal number and mean ice crystal number concentration (Figure 3a), total ice water mass and mean ice water content (Figure 3b), and ice crystal loss processes rates of a contrail cirrus cluster that is dynamically controlled (Figure 3c). Considering high soot emissions, the ice

Table 1
Summary of Simulations of Contrail Cirrus Clusters, Their Specification (M, Microphysically Control; D, Dynamically Control; and T, Transition Regime), and the Synoptic Situation at the Time of Contrail Formation for the Eight Different Cases Studies in Which Contrails Have Formed

Case study	Synoptic situation	Flight level	Initial ice crystal number concentration (cm^{-3})
1 M	ahead of a trough	220 hPa	150; 30
		260 hPa	150; 120; 90; 75; 60; 30; 10
2 M	ahead of a trough, warm and moist	220 and 260 hPa	150; 30
3 M	ahead of a weak short-wave trough	220 and 260 hPa	150; 30
4 D	ahead of a trough, large natural cloud cover	220 and 260 hPa	150; 30
5 D	zonal flow, cold and dry	220 hPa	150; 30
		260 hPa	150; 120; 90; 75; 60; 30; 10
6 T	within ridge, warm and moist	220 and 260 hPa	150; 30
7 T	within trough—ahead of ridge	220 an 260 hPa	150; 30
8 T	zonal flow, cold and dry	220 and 260 hPa	150; 30

Note. For each case study, contrails have been initialized for high soot (150 cm^{-3}) and low soot emissions (30 cm^{-3}) prescribing air traffic at 220 hPa and 260 hPa for 1 h over the eastern U.S., which results in four simulations per case study. In addition, five further reductions in the initial ice crystal number concentration (toward 120, 90, 75, 60, and 10 cm^{-3}) have been simulated for cases 1 and 5. Cases 1, 2, and 3 are classified to be microphysically controlled; cases 4 and 5 are dynamically controlled; and cases 6, 7, and 8 occur in the transition regime. The numbering of the contrail cirrus clusters does not represent the chronological order of their occurrence.

crystal loss due to dynamical processes is very large right at the beginning and amounts to about 75% within the first 2 h while the microphysical ice crystal loss is less than 3%. The rate of decrease of the ice crystal number concentration is at that time similar to that of the total ice crystal number since the increase in contrail cirrus volume and the associated dilution is relatively small in the early life cycle.

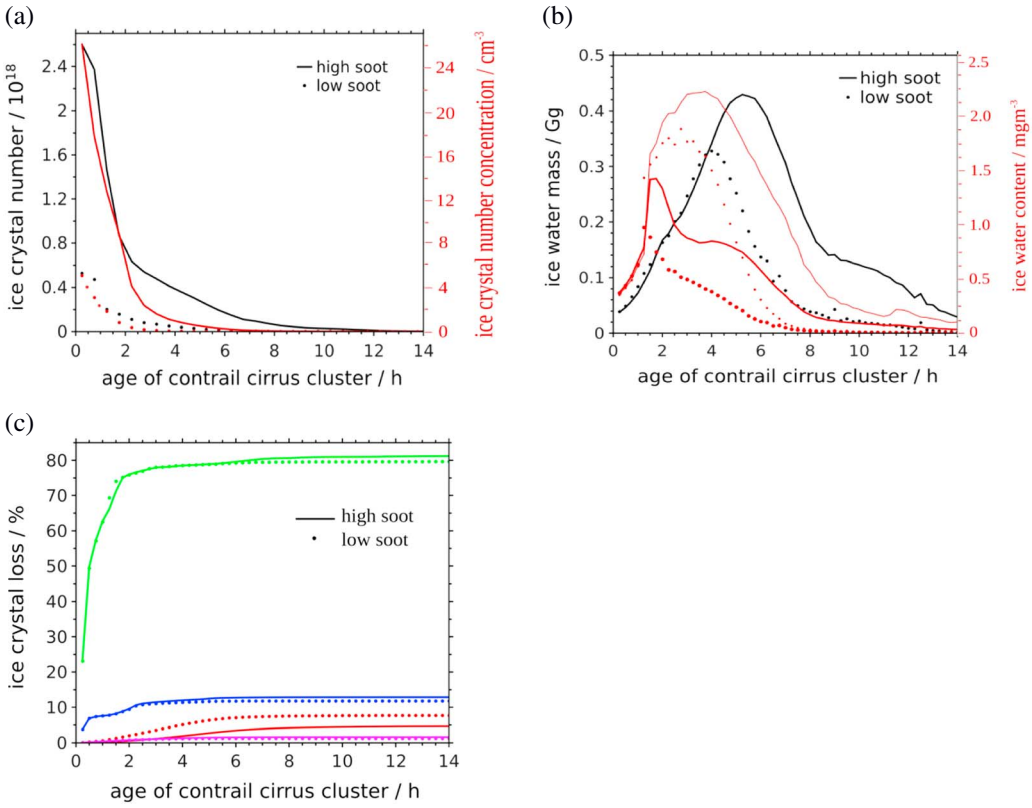

Figure 3. Contrail cirrus case study for a synoptic situation with strong dynamical control (case 5): temporal evolution of a contrail cirrus cluster with air traffic at 260 hPa showing (a) total contrail cirrus ice crystal number (black) and mean in-cloud ice crystal number concentration (red), (b) total ice water mass (black) and mean in-cloud ice water content (red) averaged over all vertical levels (thick) and only over the air traffic level (thin), and (c) accumulated ice crystal loss in percent due to sedimentation (red), precipitation (purple), dynamical processes (green), and replacement by natural cirrus (blue).The solid lines symbolize the high soot, and the dotted lines symbolize the low soot case. The contrail cirrus age indicates the time after the termination of air traffic.

Due to the large dynamical ice crystal loss rates, water deposition is extremely limited so that the total ice water mass of the contrail cirrus cluster stays very low. The maximum of ice water mass is reached after 5 h, when 95% of the initial ice crystal number has been lost already, and amounts to only about 4% of the maximum in the microphysically controlled case described above (Figure 2b). Ice water content reaches its maximum after around 1.5 h increasing by a factor of 4 relative to the beginning of the life cycle and is about 70% larger than the maximum in the microphysically controlled situation. The ice water content in the contrail core (at about flight level) is similarly strongly increased compared to the microphysically controlled case. The higher ice water content is caused by the very low sedimentation rates. This means that ice water mass is low due to the fact that many ice crystals are lost due to dynamical processes, but in the areas where contrail cirrus persist (close to a very moist region with high natural cloud coverage) deposition rates are high leading to large ice water content.

In this case, we would expect a relatively low lifetime of the contrail cirrus cluster due to the rapid loss of the ice crystals by dynamical processes. However, the ice water mass sinks below its value at the beginning of life cycle (15 min of age) after 13 h so that the contrail cirrus lifetime is approximately as large as the lifetime in the microphysically controlled case since some remnants of the former cluster persist quite long.

The reduction of soot emissions makes hardly any difference to the contrail cirrus life cycle. Integrated over the contrail cirrus life cycle, sedimentation loss rates are only about 3% higher for the low soot case. The maximum ice water mass is reached 1 h earlier and is reduced by only 25% compared to the high soot case. Largest differences can be seen in the ice water content where the maximum is decreased by 40% relative to the maximum at high soot emissions.

4.2. Variability in Sedimentation Loss

The percentage of ice crystals lost due to sedimentation is very variable (Figure 4a). In the very long lasting ice-supersaturated area described in section 3, over 40% of ice crystals are lost by sedimentation into an ice-subsaturated atmospheric layer when prescribing high soot emissions, whereas in cases 4 and 5 only around 3–5% of ice crystals are lost in this way. The fraction of ice crystals lost because of sedimentation correlates only roughly with the lifetime of the contrail cirrus cluster. The longer lived the contrail cirrus cluster (indicated by the time at which the curves flatten out), the more ice crystals tend to be lost due to sedimentation. Basically, large parts of our contrail cirrus clusters 4 and 5 (that is many contrails within) are so short-lived due to dynamical reasons that only a small fraction of ice crystals attain sizes that lead to significant sedimentation. Nevertheless, some remnant of contrail cirrus cluster 5 persists quite long so that it is difficult to estimate a suitable lifetime for this cluster. Another exception is contrail cirrus cluster 2 being quite short-lived even though microphysical processes play a large role.

Compared to the simulations prescribing low soot emissions (dotted lines), the same signature as in section 3 can be seen for all the contrail cirrus clusters. When prescribing low soot emissions the accumulated loss of ice crystals due to sedimentation grows much faster than when prescribing high soot emissions. The differences due to the change in soot emissions are large but smaller than the effect of the variability in the synoptic state. At the beginning of the life cycle, the change in the soot emissions is dominant. Even in the contrail cirrus clusters classified as belonging to the transition regime the sedimentation loss in the low soot case is significantly larger in the first few hours of the contrail cirrus life cycle than for our most favorable synoptic situation when prescribing high soot emissions.

The difference in the accumulated ice crystal loss due to sedimentation into ice-subsaturated layers between low and high soot cases (Figure 4b) is always positive varying between 3 and 16% accumulated over the whole life cycle. The larger sedimentation loss results from the ice crystal sizes being larger in low soot cases due to the reduction in the initial ice crystal number while the water vapor available for deposition stays constant. Differences in the accumulated sedimentation loss are largest for the microphysically controlled cases 1, 2, and 3 and for the transition case 7. The former display a distinct maximum of 25%, 16%, and 20%, respectively, after about 4 to 6 h. As in the life cycle of the contrail cirrus cluster described in section 3.2, the initial steep increase of the contrail cirrus volume in the low soot cases is due to the faster growth of the ice crystals and the consequently larger sedimentation rates. Later in the life cycle, differences in sedimentation loss decrease and the initially lower sedimentation loss and volume growth rates in the high soot cases are partly compensated by the larger sedimentation loss in the later contrail cirrus life cycle. At that time, after about

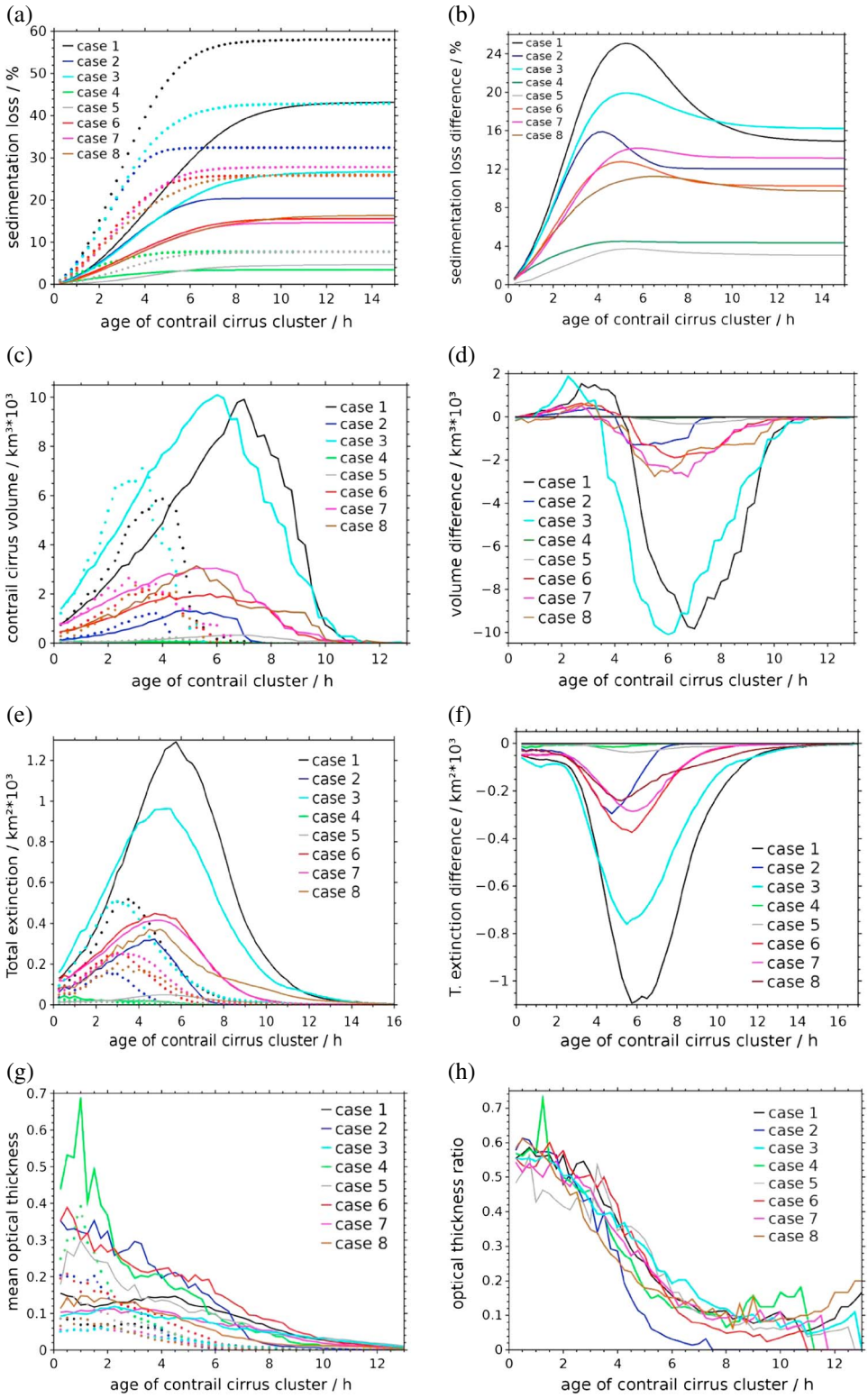

Figure 4. Temporal evolution of contrail cirrus properties for different synoptic situations with air traffic at 260 hPa showing (a and b) the ice crystal sedimentation loss accumulated over time, (c and d) volume with optical depth larger than 0.02, (e and f) the total extinction, and (g and h) the average optical depth. While Figures 4a, 4c, 4e, and 4g depict the absolute values (high soot cases solid and low soot cases dotted lines), Figures 4b, 4d, and 4f represent the difference (low minus high soot) and Figure 4h represents the ratio (low divided by high soot) between low and high soot cases. The age of the contrail cirrus cluster indicates the time after termination of air traffic. In Figure 4a, the green dotted line is partially hidden behind the grey dotted line and the red dotted line is partially hidden by the brown dotted line. The classification of the synoptic cases is given in Table 1.

Table 2
Properties of the Simulated Contrail Cirrus Clusters for the Eight Different Cases With Air Traffic at 260 hPa

Case	$VolHS_{max}$	$VolLS_{max}$	Vol_{Diff}	$ExtHS_{max}$	$ExtLS_{max}$	Ext_{Diff}	Ext_{Rel}	LT_{Diff}
1	9.91 (7)	5.87 (4)	−32.3	1.29 (5.75)	0.52 (3.5)	−5.27	72.0	−4.5
2	1.33 (4.75)	1.23 (3.75)	−2.55	0.32 (4.75)	0.16 (2.5)	−0.87	65.4	−2.5
3	10.10 (6)	6.59 (3.25)	−36.8	0.96 (5.25)	0.51 (3)	−3.88	64.5	−4
4	0.09 (0.5)	0.10 (0.5)	−0.07	0.044 (0.5)	0.027 (1)	−0.07	49.3	−2.25
5	0.32 (7)	0.24 (4.5)	−1.11	0.05 (5.25)	0.024 (4)	−0.20	64.0	−5.5
6	2.00 (5.75)	2.17 (3.5)	−5.10	0.45 (4.75)	0.26 (3)	−1.58	63.1	−3.75
7	3.05 (5.75)	2.41 (2.75)	−8.35	0.42 (5)	0.25 (3.25)	−1.28	54.0	−2.75
8	3.15 (5.25)	2.15 (3)	−8.93	0.37 (4.5)	0.19 (3)	−1.58	60.9	−4.75

Note. Maxima of contrail cirrus volume with an optical depth >0.02 in 10^3 km^3 and total extinction in 10^3 km^2 for high ($VolHS_{max}$ and $ExtHS_{max}$) and low soot cases ($VolLS_{max}$ and $ExtLS_{max}$), and the difference in volume and total extinction between low and high soot integrated over time (Vol_{Diff} and Ext_{Diff}) in 10^3 km^3 h and 10^3 km^2 h, respectively. The values in parentheses represent the corresponding age of the contrail cirrus cluster in h when the maxima occur. Ext_{Rel} represents the percentage reduction of the time-integrated total extinction due to reduced soot emissions. The last column shows the lifetime differences in h between low and high soot cases where the lifetime here is defined as the age of the contrail cirrus cluster when the normalized total extinction sinks below 0.05. The classification of the different case studies is given in Table 1.

5 h, only few ice crystals are left in the low soot case leading to the slowly decreasing sedimentation loss rates in the low soot simulations (Figure 4a), whereas in the high soot simulations water deposition on the many remaining contrail cirrus ice crystals and accordingly sedimentation rates are still large. In cases 2 and 4, the life cycle of the contrail cirrus cluster in the low soot regime seems to be nearly finished.

In the dynamically controlled cases 4 and 5, differences in the ice crystal loss due to sedimentation between low and high soot cases are much smaller, never exceeding 5%. There are no pronounced maxima in the difference of sedimentation loss. Since these contrail cirrus clusters develop in small-scale ice-supersaturated areas, many ice crystals are quickly lost due to dynamical processes and deposition rates are very low. Only a low fraction of ice particles is lost by sedimentation. In the transition regime (cases 6, 7, and 8) maximum differences in sedimentation loss range between 11% and 14%. The maxima are less pronounced than in the microphysically controlled cases, and the final differences between low and high soot cases vary between around 9% and 13%.

In order to discuss the potential of mitigating the radiative impact of contrail cirrus by reducing soot number emissions, it is essential to know how the increased sedimentation loss due to reduced soot number emissions affects the changes of contrail cirrus macrophysical and optical properties. We consider volume with optical depth larger than 0.02 (section 4.3) and total extinction (section 4.4).

4.3. Volume of Contrail Cirrus Clusters

Figure 4c shows the volume with optical depth larger than 0.02 of the contrail cirrus clusters and its temporal development for the different synoptic cases and for low and high soot emissions. The simulated evolution of contrail cirrus volume varies strongly depending on the synoptic situation. At the beginning of the contrail cirrus life cycle, the contrail cirrus volume is larger in the low soot than in the high soot cases (Figure 4d). As explained above, this is due to the initially larger sedimentation rates at low soot emissions. In the later part of the life cycles, after around 3 to 5 h, the volume of the contrail cirrus clusters with optical depth larger than 0.02 is always larger in high soot cases. This is because sufficient ice particles are still available in the high soot cases maintaining a higher ice water mass and optical depth. High soot simulations do not always attain a larger maximum contrail cirrus volume than low soot simulations (cases 4 and 7) but maxima tend to occur later.

In the microphysically controlled cases 1 and 3, the initially larger volume increase at low soot emissions and also the later volume increase at high soot emissions are largest (Figure 4d) since the contrail cirrus clusters develop in a large-scale ice-supersaturated area. The maximum volume at high soot emissions is at least 3 times larger than for all the other synoptic cases but only 1.5 to 1.7 larger than the maximum volume at reduced soot number emissions (Table 2). Hence, the synoptic situation tends to have a larger impact on the contrail cirrus volume than the reduction of soot particle emissions.

For the two synoptic cases that we classified to be almost exclusively dynamically controlled cases 4 and 5, volume increases are extremely low with maximum volumes being more than 1 order of magnitude smaller than for cases 1 and 3. This is because 85–90% of the initially formed ice particles are lost due to dynamical processes and due to replacement by natural cirrus during the first 2 h. Therefore, water deposition and contrail cirrus volume with optical depth larger than 0.02 remain low over the whole contrail cirrus life cycle. For case 2, which is classified to be microphysically controlled, the contrail cirrus volume is quite low as well, lower than in the transition cases. The maximum of contrail cirrus volume appears to be partly determined by the initial contrail volume which varies strongly as well. Given that in case 2 the initial contrail volume is only a little larger than for cases 4 and 5, the maximum volume is significantly larger than for the latter two cases. On the other hand, in case 7 the initial contrail volume is nearly as large as in case 1, but the maximum volume is less than a third of that in case 1. This means that the initial volume is a predictor for the later contrail cirrus life cycle but a large variability remains.

The integral of the difference in contrail cirrus volume over time (Table 2) is a measure for the volume reduction of the contrail cirrus cluster during the whole life cycle and therefore a first indicator for the climatic impact of the decrease in the initial ice crystal number. Integrated over the whole contrail cirrus life cycle, the contrail cirrus volume is decreased due to a reduction in soot emissions in all our case studies. Largest integrals of the volume differences occur in cases 1 and 3. The difference in the microphysically controlled case 2 is much smaller. Nevertheless, the integrated differences are on average much larger than those in the dynamically controlled cases 4 and 5. In principal, it is possible that the contrail cirrus life cycle finishes before the switchover (moving from a larger to a smaller contrail cirrus volume for reduced initial ice crystal number) happens so that reduced soot emissions would cause an increase in contrail cirrus volume integrated over the whole life cycle. We have found this behavior in one of our winter time simulations for air traffic at 220 hPa (not shown here).

Overall, it can be said that a reduction of soot emissions nearly always reduces contrail cirrus volume and therefore, cover when integrated over the whole contrail cirrus life cycle. Only in some cases, particularly in large-scale ice-supersaturated areas, this impact appears to be large enough to be directly observable.

4.4. Total Extinction

To characterize the contrail cirrus short-wave radiative impact, we need to consider volume and optical depth in combination. Contrail cirrus clusters reaching a large volume during their life cycle need not necessarily attain a high optical depth (cases 1 and 3), and clusters associated with a relatively low volume can have a large optical depth (cases 2, 4, and 6). We therefore calculate the "total extinction" (equation (1a)) choosing that quantity instead of the radiative forcing, since this makes the analysis independent of the time of day at which the contrail cirrus cluster develops.

Figure 4e shows the total extinction for the simulations with high and low soot emissions in the different synoptic systems. The total extinction maxima at high soot emissions are shifted toward shorter contrail cirrus ages by around 1 h compared to the maxima of the volume (Figure 4c). This is due to the decline in optical depth, that is commonly seen, which counteracts the impact of the increasing volume on total extinction. The increase in ice water mass, resulting from the increasing contrail cirrus volume, cannot compensate the decreasing ice crystal number concentrations. In the low soot cases, optical depth decreases even faster due to the initially larger volume increase and the associated increased dilution. In contrast to the volume, the total extinction is in all our cases larger in the high soot cases even at the beginning of the contrail cirrus life cycle (Figure 4f). This is caused by the lower initial ice crystal number concentration resulting in 40–50% lower contrail cirrus optical depths in the low soot cases than in the high soot cases within the first 2 h (Figure 4h). Reductions relative to the integrated total extinction range between 50% and 70% (Table 2) with relative reduction being not strongly dependent on the synoptic situation.

We have found one exception to the rule that integrated total extinction is always larger in high soot cases. In this case, the lifetime of the contrail cirrus cluster is so short that for low soot emissions the contrail cirrus volume and total extinction integrated over the whole life cycle are larger since the larger volume overcompensates the difference in the optical depth.

Maximum total extinction in microphysically controlled cases 1 and 3 is far larger for high than for low soot emissions, by a factor of 2.5 and 1.9, respectively (Table 2). The factors for total extinction are higher than for

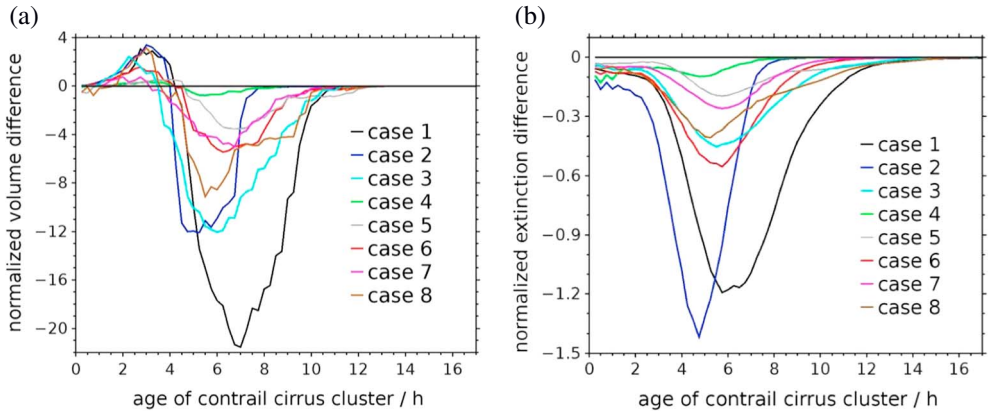

Figure 5. Difference in (a) normalized contrail cirrus volume (optical depth >0.02) and (b) normalized total extinction between low and high soot regimes (low minus high soot) for the different synoptic cases with air traffic at 260 hPa. The initial contrail volume and cover have been taken at the time of air traffic termination.

volume since the optical depth is, for reduced soot emissions, around 60 to 80% smaller at the time of maximum extinction (Figure 4h). Despite the fact that both microphysically controlled cases attain a very similar maximum contrail cirrus volume, the maximum of total extinction for case 1 is far larger than the one for case 3. This is due to the fact that the optical depth of the contrail cirrus cluster (Figure 4g) is larger in case 1 than in case 3, which is caused by larger deposition rates in case 1 particularly during the middle to latter part of the contrail cirrus life cycle. This difference in optical depth becomes clearly pronounced after about 3.5 h which is exactly the age at which the extinction starts being significantly larger than in case 3. Due to this difference in optical depth, the difference in total extinction between low and high soot emissions is also smaller for case 3 (Figure 4f). Just as for volume, the total extinction for case 2 is much lower than for cases 1 and 3. For the dynamically controlled cases, total extinction is more than an order of magnitude smaller than for the microphysically controlled cases 1 and 3.

The time-integrated difference in total extinction between high and low soot cases (Table 2) is a measure for the reduction of the shortwave radiative impact of contrail cirrus due to reduced soot number emissions. As expected from the previous results (section 4.3), the reduction of total extinction is largest for the microphysically controlled cases 1 and 3, whereas it is relatively small in case 2. The time-integrated differences are very small in the dynamically controlled cases 4 and 5.

The mean optical depth is relatively large in case 3, in particular for high soot emissions ranging between 0.4 and 0.7 in the first 2 h. The contrail cirrus cluster forms in an area where humidity is increasing strongly. Consequently, more than 50% of the ice crystals are lost due to replacement by natural cirrus within the first 2 h and large parts of the contrail cirrus cluster close to the natural cirrus experience very large deposition rates so that a high optical depth is reached.

4.5. Development Relative to Initial Volume and Cover

Differences in volume and total extinction (Figures 4d and 4f) are relatively small in the synoptic case 2 (compared to cases 1 and 3) although the contrail cirrus cluster is classified to be microphysically controlled. As noted in section 4.2 the initial contrail volume has a large impact on the later contrail cirrus volume. Therefore, we consider normalized volume and total extinction (equation (1b)) in order to characterize the development of a contrail cirrus cluster relative to its initial volume or rather cover (Figure 5).

Differences in the normalized contrail cirrus volume (Figure 5a) and normalized total extinction (Figure 5b) due to a reduction in soot emissions are large in our case 1, as expected from the previous results. In synoptic case 2, the differences in normalized volume and extinction due to soot reductions are large, while the non-normalized differences (Figure 4d and 4f) were relatively small. The normalized differences in volume (Figure 5a) increase at a similar rate and reach similar magnitudes for cases 2 and 3. The originally high difference in total extinction in case 3 is strongly reduced after normalization and turns out to be even lower than in case 2. This is because the initial contrail cover, at the time of contrail formation, is relatively low in

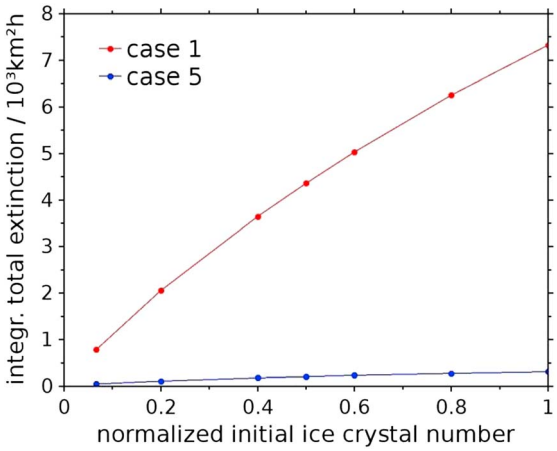

Figure 6. Time-integrated total extinction of contrail cirrus depending on the initial ice crystal number for one microphysically (case 1, red) and one dynamically controlled situation (case 5, blue). The initial ice crystal number has been normalized by $6 \cdot 10^{12}$ m^{-1}. The sensitivity study has been considered for reductions of the initial ice crystal numbers by 20%, 40%, 50%, 60%, 80%, and 93% indicated by the dots.

case 2 while the specific humidity is large leading locally to higher deposition rates and consequently higher ice water content and optical depth of the contrail cirrus cluster. The opposite is true for case 3.

This means that depending on the synoptic situation, an initially small contrail cirrus cluster (with low cover and volume), such as the one simulated for case 2 (Figure 4c), can evolve to have a large volume and short-wave radiative impact relative to its initial cover. Reducing soot emissions is therefore not only of great benefit in large-scale ice-supersaturated areas but can be also beneficial in geographically very limited areas in which a lot of water is available for deposition. One such case is represented in our case 2 showing a synoptic situation associated with a large natural cirrus coverage limiting the presence of contrail cirrus.

4.6. Lifetime

In Figures 4c and 4e the shortening of the life cycle of the contrail cirrus cluster with reduced soot emissions is visible. We here define the lifetime as the age of the contrail cirrus cluster at which the short-wave radiative impact relative to the initial cover (normalized total extinction) sinks below a certain threshold, which we have set to 0.05. Table 2 shows the lifetime differences between low and high soot cases. We find that contrail cirrus lifetime is decreased significantly, by nearly 4 h on average, due to reduced soot number emissions. We would expect a larger decrease in contrail cirrus lifetime in the microphysically controlled situations, where sedimentation loss is strongly increased due to reduced soot number emissions (Figure 4b), than in the dynamically controlled situations. However, the results do not clearly show a connection between the change in contrail cirrus lifetime and the synoptic situation. A clearer connection would be expected when analyzing the life cycle of single contrails instead of whole contrail cirrus clusters.

4.7. Sensitivity to Initial Ice Crystal Number

The time-integrated total extinction has been calculated for a number of different reductions in the initial ice crystal number, that is, by 20%, 40%, 50%, 60%, 80%, and 93%, for one microphysically and one dynamically controlled situation (Figure 6). As already indicated by the previous results, the reduction of the initial ice crystal number leads to a much stronger decrease in the short-wave radiative impact in the microphysically than in the dynamically controlled case since total extinction is very low even at high soot emissions in the latter case. A nonlinear dependency on the initial ice crystal number can be seen in both situations; that is, the decrease in time-integrated total extinction becomes stronger with decreasing initial ice crystal number. These results confirm that the use of alternative fuels has a large impact on contrail cirrus properties and radiative impact in large-scale and long-lived ice-supersaturated areas where microphysical processes are of major importance. On the other hand, the absolute change in contrail cirrus total extinction is small in the dynamically controlled contrail cirrus life cycle; only relative to the integrated total extinction the reduction is of importance (Table 2).

5. Frequency of Synoptic Situations Allowing a Large Microphysical Control

As shown above, the effect of changed soot number emissions is largest in microphysically controlled cases that typically occur in large-scale and long-lived ice-supersaturated areas. It is therefore crucial to determine how often such synoptic situations occur in which long-lived and climate-relevant contrail cirrus clusters can develop and persist.

We performed a simulation over 2 years prescribing air traffic over the eastern U.S. at 220 hPa every 28 h for 1 h only resulting in slightly more than 600 synoptic case studies. We classified the contrail cirrus life cycles depending on the synoptic situation as introduced in section 3.2.

Twenty-six percent of the cases are microphysically controlled, while contrail cirrus clusters are clearly dynamically controlled in about 34% of the synoptic situations. The transition regime occurs in 27% of the cases

and in the remaining situations (13%) contrails did not form. There is a slight tendency for microphysically controlled clusters to be more common in summer.

We point out that the frequencies of occurrence of ice supersaturation and of microphysically controlled contrail cirrus clusters are likely to be dependent on the exact location with a higher probability of large-scale ice-supersaturated areas in the main storm track areas. We selected the area over the eastern U.S. since this is an area where many contrail cirrus outbreaks occur (Carleton et al., 2008).

6. Summary and Conclusions

In this paper, we study the life cycle of contrail cirrus clusters and their modification due to reduced soot number emissions approximated by reduced initial ice crystal numbers. It is known that contrail cirrus cover is highly variable depending on the synoptic situation and that contrail cirrus cover is largely made of a few long-lived contrail cirrus clusters (e.g., Burkhardt & Kärcher, 2009). Here we study the large variability of the life cycle of several contrail cirrus clusters, the processes responsible for this variability, and their dependence on the synoptic situation. Furthermore, we study the influence of reduced initial ice crystal numbers on contrail cirrus properties, life cycle, and short-wave radiative forcing. Exemplarily, we investigate in detail a large reduction by 80% and explore the sensitivity to the size of the reduction. We analyze which processes are responsible for a decrease in ice crystal numbers and how the volume and associated total extinction of the contrail cirrus clusters evolve over the life cycle. We analyze the development of contrail cirrus clusters originating over the eastern U.S. regarding their microphysical and macrophysical properties. We choose the eastern U.S. for our experiments since it is one of the peak air traffic areas in the midlatitudes and since contrail cirrus outbreaks are frequently seen over the eastern U.S.

In a large-scale and long-lived ice-supersaturated area, a contrail cirrus cluster was shown to attain a contrail cirrus volume that is several times larger than the volume a few minutes after formation. In this synoptic situation, maximum volume (connected with optical depth >0.02) and ice water mass were reached after about 7 h when ice crystal number had decreased to about a sixth of its original value. Since the contrail cirrus cluster has developed in a particularly humid, long-lived, and large-scale ice-supersaturated area, a large fraction of the ice crystals surviving the vortex phase (more than 40%) is lost due to sedimentation of ice crystals into ice-subsaturated areas. Investigating contrail cirrus life cycles in 10 different synoptic situations in winter, we find a large variability of contrail cirrus life cycles with some barely growing in terms of contrail cirrus volume and others displaying a great potential for growth. Contrail cirrus clusters whose life cycles are microphysically controlled (accumulated sedimentation loss of ice crystals $>20\%$) typically occur in long-lived and large-scale ice-supersaturated areas, for example, ahead of troughs and dynamically controlled contrail cirrus clusters generally develop in short-lived and small-scale ice-supersaturated areas. Those contrail cirrus clusters developing in large-scale ice-supersaturated areas tend to be long-lived and climate-relevant in terms of their total extinction.

The volume of contrail cirrus with associated optical depth >0.02 is initially larger for low soot emissions since fewer ice crystals are initially formed which leads to a larger sedimentation rate. This initial increase in contrail cirrus volume is reinforced by a stronger tilting of the contrails which again causes a larger volume increase due to sedimentation. This larger contrail cirrus volume is connected with larger deposition rates, a faster increase in total ice water mass within the contrail cirrus volume and consequently with enhanced ice crystal loss due to sedimentation. The larger ice crystal number in the high soot cases results in an increased optical depth outweighing the smaller contrail cirrus volume at the beginning of the life cycle. The volume of the contrail cirrus clusters with optical depth larger than 0.02 starts being larger in the high soot than in the low soot cases after about 4 h unless the life cycle is terminated before this can happen. This is because sufficient ice crystals are still available in the high soot cases maintaining a higher ice water mass and both together causing a relatively high optical depth. Total extinction is usually larger for high soot emissions during the whole life cycle because of the much larger ice crystal number concentration. It is reduced by about 50% to 70% due to the 80% decrease in initial ice crystal numbers. The variability in this reduction is not clearly attributable to the differences in synoptic situations. The reduction of soot number emissions leads on average to a contrail cirrus lifetime decrease by around 4 h.

The effect of reduced soot number emissions is largest in the microphysically controlled cases where the ice crystal loss due to sedimentation is increased by about 15%. The volume of the contrail cirrus cluster,

exceeding an optical depth of 0.02, and total extinction integrated over time are strongly decreased due to reduced soot emissions in particular in the microphysically controlled cases. Since the contrail cirrus volume and total extinction depend on the initially formed contrail volume, this reduction may in some cases only be visible once volume and total extinction are normalized with the initially formed contrail volume and cover, respectively. This implies that the impact of reduced soot number emissions can also be large for small contrail cirrus clusters at least relative to the initially formed contrail volume or cover. Contrail cirrus volume integrated over the contrail cirrus life cycle is nearly always reduced due to a reduction in soot emissions, but only in some cases, in particular in large-scale ice-supersaturated areas, we would expect this impact to be observable. The effect of reduced soot number emissions is lowest in the synoptic situations where contrail cirrus clusters are dynamically controlled. The increase of ice crystal loss due to sedimentation remains below 5%. The decrease in volume and total extinction is very low as well.

Reductions in the initial ice crystal number by 20%, 40%, 50%, 60%, 80%, and 93% confirm the large impact of decreased soot number emissions in microphysically controlled contrail cirrus life cycles. In addition, a nonlinear dependency on the initial ice crystal number can be seen in the short-wave radiative impact by contrail cirrus.

We expect our results to be representative for the extratropics, in particular for the main baroclinic zones which are characterized by storm track activity and large frontal zones. In the tropics, the dynamics lead to ice-supersaturated areas with very different spatial and temporal scales so that our results cannot be transferred to these areas.

We estimate that contrail cirrus clusters whose life cycles are microphysically controlled occur in about 25% of cases over the eastern U.S. This means that long-lived and climate-relevant contrail cirrus clusters associated with a high optical depth or coverage do occur frequently in this area. The frequency may depend on whether we study synoptic situations within or outside the main storm track areas. Nevertheless, within the main air traffic areas of the extratropics, the use of alternative fuels appears to be an efficient means for mitigating the contrail cirrus climate impact significantly.

Our analysis is somewhat limited, on the one hand, by the low resolution of the model and the bulk microphysical scheme and, on the other hand, by the fact that we cannot estimate the change in the global contrail cirrus climate impact from our simulations of contrail cirrus clusters. We encourage conducting high-resolution simulations in order to analyze the variability of contrail cirrus life cycles and their connection with the synoptic evolution in more detail. Furthermore, the increased process understanding from our life cycle studies lends itself to the interpretation of global climate simulations of the impact of reduced initial ice crystal number concentrations.

Acknowledgments
The authors thank Michael Ponater, Simon Unterstrasser, and three anonymous reviewers for their helpful comments. The presented data are available at https://www.pa.op.dlr.de/opendata/JGR-2017JD027011R. This work was funded by the DLR project ECLIF (Emission and CLimate Impact of alternative Fuels). Computational resources were made available by the German Climate Computing Centre (DKRZ) trough support from the German Federal Ministry of Education and Research.

References

Beyersdorf, A. J., Timko, M. T., Ziemba, L. D., Bulzan, D., Corporan, E., Herndon, S. C., … Anderson, B. E. (2014). Reductions in aircraft particulate emissions due to the use of Fischer–Tropsch fuels. *Atmospheric Chemistry and Physics*, *14*(1), 11–23.

Bock, L., & Burkhardt, U. (2016a). The temporal evolution of a long-lived contrail cirrus cluster: Simulations with a global climate model. *Journal of Geophysical Research: Atmospheres*, *121*(7), 3548–3565. https://doi.org/10.1002/2015JD024475

Bock, L., & Burkhardt, U. (2016b). Reassessing properties and radiative forcing of contrail cirrus using a global climate model. *Journal of Geophysical Research: Atmospheres*, *121*(16), 9717–9736. https://doi.org/10.1002/2016JD025112

Bond, T. C., Doherty, J., Fahey, D. W., Forster, P. M., Berntsen, T., De Angelo, B. J., … Zender, C. S. (2013). Bounding the role of black carbon in the climate system—A scientific assessment. *Journal of Geophysical Research: Atmospheres*, *118*(11), 5380–5552. https://doi.org/10.1002/jgrd.50171

Boucher, O., Randall, D., Artaxo, P., Bretherton, C., Feingold, G., Forster, P., … Zhang, X. (2013). Clouds and aerosols. In T. Stocker, et al. (Eds.), *Climate change 2013: The physical science basis. Contribution of working group I to the Fifth Assessment Report of the Intergovernmental Panel on Climate Change* (Vol. 7, pp. 571–658). Cambridge, UK, and New York: Cambridge University Press.

Burkhardt, U., & Kärcher, B. (2009). Process-based simulation of contrail cirrus in a global climate model. *Journal of Geophysical Research*, *114*, D16201. https://doi.org/10.1029/2008JD011491

Burkhardt, U., & Kärcher, B. (2011). Global radiative forcing from contrail cirrus. *Nature Climate Change*, *1*(1), 54–58.

Burkhardt, U., Kärcher, B., Ponater, M., Gierens, K., & Gettelman, A. (2008). Contrail cirrus supporting areas in model and observations. *Geophysical Research Letters*, *35*, L16808. https://doi.org/10.1029/2008GL034056

Carleton, A. M., Travis, D. J., Master, K., & Vezhapparambu, S. (2008). Composite atmospheric environments of jet contrail outbreaks for the United States. *American Meteorological Society*, *47*, 641–667.

Carlson, T. N. (1991). *Mid-latitude weather Systems* (pp. 507). London-New York: Harper Collins Academic.

Chen, C.-C., & Gettelman, A. (2013). Simulated radiative forcing from contrails and contrail cirrus. *Atmospheric Chemistry and Physics*, *13*(24), 12,525–12,536.

Duda, D., Minnis, P., Khlopenkov, K., Chee, T., & Boeke, R. (2013). Estimation of 2006 Northern Hemisphere contrail coverage using MODIS data. *Geophysical Research Letters*, *40*(3), 612–617. https://doi.org/10.1002/grl.50097

Duda, D., Minnis, P., & Nguyen, L. (2001). Estimates of cloud radiative forcing in contrail clusters using GOES imagery. *Journal of Geophysical Research*, *106*(D5), 4927–4937.

Duda, D., Minnis, P., Nguyen, L., & Palikonda, R. (2004). A case study of the development of contrail clusters over the Great Lakes. *Journal of the Atmospheric Sciences*, *61*(10), 1132–1146.

Eyers, C., Norman, P., Middel, J., Plohr, M., Michot, S., Atkinson, K., & Christou, R. (2004). AERO2K global aviation emissions inventories for 2002 and 2025, *Tech. Rep*., QINETIC/04/01113, QinetiQ, Farnborough, UK.

Febvre, G., Gayet, J., Minikin, A., Schlager, H., Shcherbakov, V., Jourdan, O., … Schumann, U. (2009). On optical and microphysical characteristics of contrails and cirrus. *Journal of Geophysical Research*, *114*, D02204. https://doi.org/10.1029/2008JD010184

Gierens, K., & Brinkop, S. (2012). Dynamical characteristics of ice-supersaturated regions. *Atmospheric Chemistry and Physics*, *12*(24), 11,933–11,942. https://doi.org/10.5194/acp-12-11933-2012

Grewe, V., Bock, L., Burkhardt, U., Dahlmann, K., Gierens, K., Hüttenhofer, L., … Levy, Y. (2016). Assessing the climate impact of the AHEAD multi-fuel blended wing body. *Met. Z.* https://doi.org/10.1127/metz/2016/0758

Haywood, J. M., Allan, R. P., Bornemann, J., Forster, P. M., Francis, P. N., Milton, S., … Thorpe, R. (2009). A case study of the radiative forcing of persistent contrails evolving into contrail-induced cirrus. *Journal of Geophysical Research*, *114*, D24201. https://doi.org/10.1029/2009JD012650

Heymsfield, A., & Iaquinta, J. (2000). Cirrus crystal terminal velocities. *Journal of the Atmospheric Sciences*, *57*(7), 916–938.

Heymsfield, A. J., Lawson, R. P., & Sachse, G. W. (1998). Growth of ice crystals in a precipitating contrail. *Geophysical Research Letters*, *25*(9), 1335–1338.

International Civil Aviation Organization (2007). Environmental report 2007, Environmental Unit of the International Civil Aviation Organization.

Irvine, E. A., Hoskins, B. J., & Shine, K. P. (2012). The dependence of contrail formation on the weather pattern and altitude in the North Atlantic. *Geophysical Research Letters*, *39*, L12802. https://doi.org/10.1029/2012GL051909

Irvine, E. A., Hoskins, B. J., & Shine, K. P. (2014). A Lagrangian analysis of ice-supersaturated air over the North Atlantic. *Journal of Geophysical Research: Atmospheres*, *119*(1), 90–100. https://doi.org/10.1002/2013JD020251

Kärcher, B., Burkhardt, U., Bier, A., Bock, L., & Ford, I. J. (2015). The microphysical pathway to contrail formation. *Journal of Geophysical Research: Atmospheres*, *120*(15), 7893–7927.

Kärcher, B., Burkhardt, U., Unterstrasser, S., & Minnis, P. (2009). Factors controlling contrail cirrus optical depth. *Atmospheric Chemistry and Physics*, *9*(16), 6229–6254.

Kärcher, B., Peter, T., Biermann, U. M., & Schumann, U. (1996). The initial composition of jet condensation trails. *Journal of the Atmospheric Sciences*, *53*(21), 3066–3083.

Kärcher, B., & Yu, F. (2009). Role of aircraft soot emissions in contrail formation. *Geophysical Research Letters*, *36*, L01804. https://doi.org/10.1029/2008GL036649

Kästner, M., Meyer, R., & Wendling, P. (1999). Influence of weather conditions on the distribution of persistent contrails. *Meteorological Applications*, *6*(3), 261–271.

Koop, T., Luo, B. P., Tsias, A., & Peter, T. (2000). Water activity as the determinant for homogeneous ice nucleation in aqueous solutions. *Nature*, *406*(6796), 611–614.

Kurz, C. (2007). Entwicklung und Anwendung eines gekoppelten Klima-Chemie-Modellsystems: Globale Spurengastransporte und chemische Umwandlungsprozesse, Doctoral thesis, Ludwigs-Maximilians-Universität München, München, Germany, *DLR Forschungsbericht 2007–12*. Retrieved from https://edoc.ub.uni-muenchen.de/4804/

Lamquin, N., Stubenrauch, C., Gierens, K., Burkhardt, U., & Smit, H. (2012). A global climatology for upper-tropospheric ice supersaturation occurrence inferred from the atmospheric infrared sounder calibrated by MOZAIC. *Atmospheric Chemistry and Physics*, *12*(1), 381–405.

Lee, D., Fahey, D., Forster, P., Newton, P., Wit, R., Lim, L., … Sausen, R. (2009). Aviation and global climate change in the 21st century. *Atmospheric Environment*, *43*(22-23), 3520–3537.

Levkov, L., Rockel, B., Kapitza, H., & Raschke, E. (1992). 3D mesoscale numerical studies of cirrus and stratus clouds by their time and space evolution. *Beitraege zur Physik der Atmosphaere*, *65*, 35–58.

Lewellen, D. C., Meza, O., & Huebsch, W. W. (2014). Persistent contrails and contrail cirrus. Part I: Large-eddy simulations from inception to demise. *Journal of the Atmospheric Sciences*, *71*(12), 4399–4419. https://doi.org/10.1175/JAS-D-13-0316.1

Lin, Y. L., Farley, R. D., & Orville, H. D. (1983). Bulk parameterization of the snow field in a cloud model. *Journal of Climate and Applied Meteorology*, *22*(6), 1065–1092.

Lohmann, U., Spichtinger, P., Heidt, S., Peter, T., & Smit, H. (2008). Cirrus clouds and ice supersaturation regions in a global climate model. *Environmental Research Letters*, *3*, 045022(4).

Marquart, S., Ponater, M., Mager, F., & Sausen, R. (2003). Future development of contrail cover, optical depth, and radiative forcing: Impacts of increasing air traffic and climate change. *Journal of Climate*, *16*(17), 2890–2904.

Meerkötter, R., Schumann, U., Doelling, D. R., Minnis, P., Nakajima, T., & Tsushima, Y. (1999). Radiative forcing by contrails. *Annales de Geophysique*, *17*(8), 1080–1094.

Minnis, P., Bedka, S., Duda, D., Bedka, K., Chee, T., Ayers, J., … Boeke, R. (2013). Linear contrail and contrail cirrus properties determined from satellite data. *Geophysical Research Letters*, *40*(12), 3220–3226. https://doi.org/10.1002/grl.50569

Moore, R. H., Shook, M., Beyersdorf, A., Corr, C., Herndon, S., Knighton, W. B., … Anderson, B. E. (2015). Influence of jet fuel composition on aircraft engine emissions: A synthesis of aerosol emissions data from the NASA APEX, AAFEX and ACCESS missions. *ACS*, *29*(4), 2591–2600. https://doi.org/10.1021/ef502618w

Moore, R. H., Thornhill, K. L., Weinzierl, B., Sauer, D., D'Ascoli, E., Kim, J., … Anderson, B. E. (2017). Biofuel blending reduces particle emissions from aircraft engines at cruise conditions. *Nature*, *543*(7645), 411–415. https://doi.org/10.1038/nature21420

Murakami, M. (1990). Numerical modeling of dynamical and microphysical evolution of an isolated convective cloud—The 19 July 1981 CCOPE cloud. *Journal of the Meteorological Society of Japan*, *68*(2), 107–128.

Myhre, G., Kvalevag, M., Rädel, G., Cook, J., Shine, K. P., Clark, H., … Rodriguez de Leon, R. (2009). Intercomparison of radiative forcing calculations of stratospheric water vapour and contrails. *Meteorologische Zeitschrift*, *18*(6), 585–596.

Newinger, C., & Burkhardt, U. (2012). Sensitivity of contrail cirrus radiative forcing to air traffic scheduling. *Journal of Geophysical Research*, *117*, D10205. https://doi.org/10.1029/2011JD016736

Palikonda, R., Minnis, P., Duda, D., & Mannstein, H. (2005). Contrail coverage derived from 2001 AVHRR data over continental United States of America and surrounding areas. *Meteorologische Zeitschrift*, *14*(4), 525–536.

Paoli, R., & Shariff, K. (2016). Contrail modeling and simulation. *Annual Review of Fluid Mechanics*, *48*(1), 393–427. https://doi.org/10.1146/annurev-fluid-010814-013619

Petzold, A., Busen, R., Schröder, F. P., Baumann, R., Kuhn, M., Ström, J., … Schumann, U. (1997). Near-field measurements on contrail properties from fuels with different sulfur content. *Journal of Geophysical Research*, *102*(D25), 29867–29880.

Picot, J., Paoli, R., Thouron, O., & Cariolle, D. (2015). Large-eddy simulation of contrail evolution in the vortex phase and its interaction with atmospheric turbulence. *Atmospheric Chemistry and Physics*, *15*(13), 7369–7389. https://doi.org/10.5194/acp-15-7369-2015

Roeckner, E., Baeuml, G., Bonaventura, L., Brokopf, R., Esch, M., Giorgetta, M., … Tompkins, A. (2003). The atmospheric general circulation model ECHAM5. Part 1: Model description, *Max-Planck-Inst. Report* (Vol. 349, 127 pp.). Hamburg, Germany.

Roeckner, E., Brokopf, R., Esch, M., Giorgetta, M., Hagemann, S., Kornblueh, L., … Schulzweida, U. (2006). Sensitivity of simulated climate to horizontal and vertical resolution in the ECHAM5 atmosphere model. *Journal of Climate*, *19*(16), 3771–3791.

Rojo, C., Vancassel, X., Mirabel, P., Ponche, J. L., & Garnier, F. (2015). Impact of alternative jet fuels on aircraft-induced aerosols. *Elsevier Ltd.*, *144*, 335–341.

Schröder, F., Kärcher, B., Duroure, C., Ström, J., Petzold, A., Gayet, J., … Borrmann, S. (2000). On the transition of contrails into cirrus clouds. *Journal of the Atmospheric Sciences*, *57*(4), 464–480.

Schumann, U. (1996). On conditions for contrail formation from aircraft exhausts. *Met. Z.*, *5*, 4–23.

Schumann, U. (2002). Contrail cirrus. In D. K. Lynch, et al. (Eds.), *Cirrus* (pp. 231–255). New York: Oxford University Press.

Schumann, U. (2005). Formation, properties and climatic effects of contrails. *Comptes Rendus Physique*, *6*(4-5), 549–565.

Schumann, U., Penner, J. E., Chen, Y., Zhou, C., & Graf, K. (2015). Dehydration effects from contrails in a coupled contrail-climate model. *Atmospheric Chemistry and Physics*, *15*(19), 11179–11199. https://doi.org/10.5194/acp-15-11179-2015

Speth, R. L., Rojo, C., Malina, R., & Barrett, S. R. H. (2015). Black carbon emissions reductions from combustion of alternative jet fuels. *Elsevier Ltd.*, *105*, 37–42.

Spichtinger, P., & Gierens, K. (2009). Modelling of cirrus clouds—Part 1: Model description and validation. *Atmospheric Chemistry and Physics*, *9*(2), 685–706.

Stier, P., Feichter, J., Kinne, S., Kloster, S., Vignati, E., Wilson, J., … Petzold, A. (2005). The aerosol-climate model ECHAM5-HAM. *Atmospheric Chemistry and Physics*, *5*(4), 1125–1156. https://doi.org/10.5194/acp-5-1125-2005

Sundqvist, H. (1978). A parameterization scheme for non-convective condensation including prediction of cloud water content. *Quarterly Journal of the Royal Meteorological Society*, *104*(441), 677–690.

Unterstrasser, S. (2016). Properties of young contrails—A parametrisation based on large-eddy simulations. *Atmospheric Chemistry and Physics*, *16*(4), 2059–2082. https://doi.org/10.5194/acp-16-2059-2016

Unterstrasser, S., & Gierens, K. (2010a). Numerical simulations of contrail-to-cirrus transition—Part 1: An extensive parametric study. *Atmospheric Chemistry and Physics*, *10*(4), 2017–2036.

Unterstrasser, S., & Gierens, K. (2010b). Numerical simulations of contrail-to-cirrus transition—Part 2: Impact of initial ice crystal number, radiation, stratification, secondary nucleation and layer depth. *Atmospheric Chemistry and Physics*, *10*(4), 2037–2051. https://doi.org/10.5194/acp-10-2037-2010

Vazquez-Navarro, M., Mannstein, H., & Kox, S. (2015). Contrail life cycle and properties from 1 year of MSG/SEVIRI rapid-scan images. *Atmospheric Chemistry and Physics*, *15*(15), 8739–8749.

Voigt, C., Schumann, U., Jurkat, T., Schäuble, D., Schlager, H., Petzold, A., … Dörnbrack, A. (2010). In-situ observations of young contrails—Overview and selected results from the CONCERT campaign. *Atmospheric Chemistry and Physics*, *10*(18), 9039–9056.

Williams, K. D., & Webb, M. J. (2009). A quantitative performance assessment of cloud regimes in climate models. *Climate Dynamics*, *33*(1), 141–157. https://doi.org/10.1007/s00382-008-0443-1

Zhang, Y., Macke, A., & Albers, F. (1999). Effect of crystal size spectrum and crystal shape on stratiform cirrus radiative forcing. *Atmospheric Research*, *52*(1-2), 59–75.